Nematic-Field-Driven Positioning of Particles in Liquid Crystal Droplets

Jonathan K. Whitmer,[1,2] Xiaoguang Wang,[1] Frederic Mondiot,[1] Daniel S. Miller,[1]
Nicholas L. Abbott,[1] and Juan J. de Pablo[3,2]

[1]*Department of Chemical and Biological Engineering, University of Wisconsin-Madison, Madison, Wisconsin 53706-1691, USA*
[2]*Argonne National Laboratory, Argonne, Illinois 60349, USA*
[3]*Institute for Molecular Engineering, University of Chicago, Chicago, Illinois 60637, USA*

(Received 26 April 2013; revised manuscript received 6 September 2013; published 26 November 2013)

Common nematic oils, such as 5CB, experience planar anchoring at aqueous interfaces. When these oils are emulsified, this anchoring preference and the resulting topological constraints lead to the formation of droplets that exhibit one or two point defects within the nematic phase. Here, we explore the interactions of adsorbed particles at the aqueous interface through a combination of experiments and coarse-grained modeling, and demonstrate that surface-active particles, driven by elastic forces in the droplet, readily localize to these defect regions in a programmable manner. When droplets include two nanoparticles, these preferentially segregate to the two poles, thereby forming highly regular dipolar structures that could serve for hierarchical assembly of functional structures. Addition of sufficient concentrations of surfactant changes the interior morphology of the droplet, but pins defects to the interface, resulting in aggregation of the two particles.

DOI: 10.1103/PhysRevLett.111.227801 PACS numbers: 61.30.Jf, 61.30.Pq, 64.75.Yz

Liquid crystals (LCs) exhibit thermodynamic and structural properties that are intermediate between those expected from ordinary solid and liquid states. Though structurally liquid, molecules within LCs can adopt distinct orientations, resulting in a new palette of technologically useful phases. Spherical confinement of LCs results in two primary morphologies. Bipolar droplets are formed when LCs prefer to order tangent to the interface (planar anchoring), creating two point defects (boojums) on their surfaces as a consequence of the Poincaré–Hopf theorem [1]. Radial morphologies appear when LC molecules are oriented perpendicular to the interface (homeotropic anchoring). A single ring- or pointlike defect is formed in the center of the droplet, with molecules outside the core aligning with the local radial vector. Uniform, axial, and uniaxial morphologies can also be achieved by tuning the anchoring strength [2,3].

Recent work has demonstrated that the tight interplay between a droplet's interface and its interior can lead to the formation of new ordered phases [4]. In such phases, the droplet interior organizes adsorbates at the interface, while the adsorbates also influence the order adopted by the LC. When a critical adsorbate concentration is reached, not only does the interior morphology of the droplet change from bipolar to homeotropic, but spherical or striped adsorbate domains also self-organize on the surface due to the interplay of enthalpy and elastic stresses. The question addressed in this Letter, which from a practical perspective is more intriguing, is whether the interior morphology of a LC droplet can be used to control the positioning of small particles at the droplet's interface. If possible, the resulting nanoparticle-decorated droplets would provide a promising new route for templated assembly of functional patchy particles [5], as well as for development of primed sensing devices, whose morphology is balanced on a knife's edge to be swayed by vanishing concentrations of analyte [6].

Small particles or impurities in a nematic LC are known to exhibit a preference for phase boundaries and defect regions [7]. In pioneering experiments on bulk LC emulsions, optical traps were utilized to demonstrate the affinity between colloidal particles and a locally melted nematic phase [8,9]. Further work has shown colloidal particles to have an affinity for disclination lines, useful in templated nanowire assembly [7,10–14]. Defect affinity, combined with self assembly of surfactant molecules, is thought to be partly responsible for the exquisite sensitivity of droplet biosensors [6,15]. While recent investigations of nematic double-emulsions [16] also indicate that an intricate interplay exists between defects on the interior and exterior droplets, studies of nanoparticles at LC droplet interfaces are not available.

Experimentally, we observe this behavior for larger droplet–particle combinations. Figure 1 shows a series of micrographs for bare [Figs. 1(a) and 1(b)] 5CB droplets and those decorated with one [Figs. 1(f)–1(h)] or two [Figs. 1(k)–1(m)] fluorescent polystyrene particles. Additional details regarding the experimental system are provided in the Supplemental Material (SM) [17]. Images generated using bright-field, polarized light, and fluorescence microscopy reveal the interior morphology of the droplet and the presence of particles at the defects. The forces holding these particles are strong—particles never leave their adopted defect unless the LC is heated through the clearing point.

To address the origin and strength of these forces, we implement a molecular model utilizing a Gay–Berne (GB)

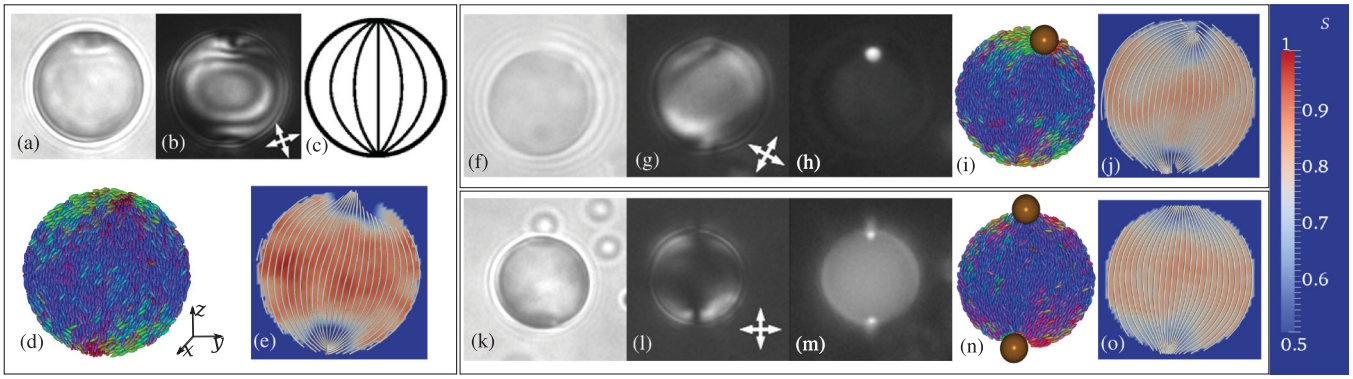

FIG. 1 (color). Experimental images of 5CB droplets in water emulsions with zero (a),(b), one (f)–(h), or two (k)–(m) adsorbed polystyrene particles. Bright-field, polarized light and fluorescence images (particle cases only) are shown alongside simulated systems depicting a $\sigma = 10\sigma_0$ particle adsorbed onto a Gay-Berne droplet of radius $R = 25\sigma_0$. Mesogens are colored by an (r,g,b) value representing their (x, y, z) orientation. The cartoon in (c) depicts the field lines expected in a bipolar morphology. (d) Snapshot of a bare droplet with planar anchoring, alongside a plot of the scalar order parameter (S) [17] and field lines within the droplet (e). The axes are given next to this plot for clarity; subsequent views are rotated, but preserve the (r,g,b) color mapping. The boojum defects are clearly visible for their low value of S and as confluence points for the field lines. For clarity, field lines are projected onto the viewing plane. Importantly, it can be seen that the defect is $\approx 5\sigma_0$ in radius. Simulation results for a single adsorbed particle (i),(j), and two adsorbed particles (n),(o) are also shown. The region of disorder within these droplets (prior to the adsorption of particles) coincides exactly with the particle positions. Overall nematic ordering is similar in each case, suggesting each configuration minimizes the LC elastic cost. In both simulation and experiment, the particles are approximately the size of the defect core. The order parameter scale for maps (e),(j),(o) is given on the right panel.

representation of the LC [17–21], with particles modeled by spheres of varying diameter. As the GB ellipsoids represent single molecules, this necessarily examines smaller length scales than those accessible in the experiments, and serves to provide a comprehensive view of particles in LC droplets that encompasses mesoscopic and microscopic length scales. Comparison between the two is justified provided the two systems exhibit the same morphology, as the driving forces in colloidal aggregation will be elastic stresses associated with the presence of defects. In the following discussion, lengths are reduced by the ellipsoid minor diameter σ_0, energies by the Gay–Berne interaction strength ε, and masses by the mesogen mass m [22]; this sets a natural timescale at $t_0 = \sqrt{m\sigma_0^2/\varepsilon}$. Anchoring and particle confinement inside a drop of radius $R = 25$ are handled by a modified 9-3 Lennard-Jones wall [17,23], which enforces a spherical shape to mimic that of larger aqueous droplets. Our approach differs from that in recent investigations of LC droplets in equilibrium with their own vapor, which adopt tactoid shapes [24,25]. We explicitly aim to avoid these geometries, and use our results for spherical geometries to connect with experiments on spherical droplets an order of magnitude larger [26], which are prohibitive to molecular simulation. Note that past work has indeed shown that results for GB systems at small length scales can be mapped onto those of continuum models at much longer length scales [27]. Additional details are provided in the SM [17].

After evolving the droplet interior to its equilibrium nematic configuration through NVT molecular dynamics simulations, we place a particle near the surface, at a radius $r = 23$, deleting any overlapping mesogens. This is done for two types of configurations: polar placement (where the particle is placed at a boojum defect), and equatorial placement (between the two boojums). Following this, two types of simulations are performed to probe dynamic and thermodynamic behavior. The dynamics are monitored for $2 \times 10^5 t_0$ in standard NVT molecular dynamics. Slow diffusion renders simple MD insufficient to sample free energies, hence, free energies are calculated through a biased molecular dynamics approach [17].

Representative configurations for particles of diameter $\sigma = 10$ placed on the surface of a droplet are given alongside the experimental images in Fig. 1 [28]. Mixing rules for the GB potential [29,30] imply planar anchoring is energetically preferred, though the actual anchoring for large particles ($\sigma \in \{8, 10\}$) is closer to homeotropic [cf. Figs. 1(i) and 1(n)]. High-splay regions are eliminated [cf. Fig. 1(e)] when a particle is located at a boojum defect, indicating that a strong preference should exist for this region. When a particle occupies this state, the disorder and elastic stress associated with the defect are eliminated. Importantly, for the $\sigma = 10$ particle depicted in the figure, the particle and boojum sizes are nearly equal. The competition in boundary conditions between particle LC and surface LC may even be enough to deform the droplet into a more elongated object to balance surface tension [31], though the rigid boundaries here prevent this. Smaller particles exhibit more planarlike orientation [29,32]. A combination of entropic and anchoring effects also limits configurations available to the particle. In simulation,

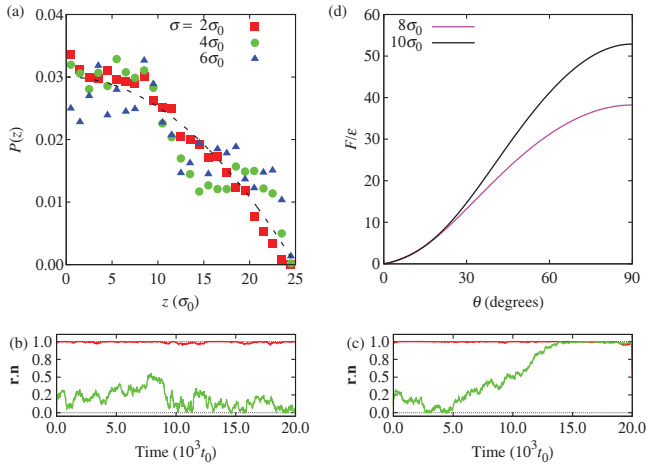

FIG. 2 (color). (a) Probability distribution for particles as a function of distance along the nematic axis $\hat{\mathbf{n}} = \hat{\mathbf{z}}$ from standard NVT simulation trajectories. The poles of the droplet are located at $z = 25$ and $z = -25$, respectively. The distribution trends toward polar regions as the particle size is increased. Statistics are coarsened by slow diffusion for large particles, which are not shown for clarity. The dashed line corresponds to a uniform volume distribution. (b),(c) Representative trajectories from simulations with (b) $\sigma = 8\sigma_0$ and (c) $\sigma = 10\sigma_0$. Red lines denote trajectories which start at a boojum defect, while green lines denote trajectories originating from the equator of the droplet. A distinct preference for the boojum region is observed in both cases. The $\sigma = 10\sigma_0$ particle segregates to one of the boojums through rotation of the nematic vector, while the $\sigma = 8\sigma_0$ particle remains in its initial misaligned configuration. (d) Potential of mean force for particles of size $\sigma = 8\sigma_0$ and $\sigma = 10\sigma_0$ as a function of the angle θ formed by the particle's radial position and the nematic axis. As the particle size increases, a deep minimum develops at the location of the boojum defects.

larger particles ($\sigma \in \{8, 10\}$) were observed primarily at the droplet interface, while smaller particles roamed the entire droplet volume.

This behavior is apparent from results shown in Fig. 2(a), where a histogram of particle positions (obtained from standard NVT molecular dynamics simulations of length $2 \times 10^5 t_0$) is plotted. Simulations were prepared by placing a particle at the interface of the droplet and allowing it to diffuse around the droplet. Note that a uniform distribution over the volume of the droplet would be proportional to $(R^2 - z^2)$, which corresponds to the dotted line. These histograms are averaged over a set of six independent simulations; three having initial conditions near the equator, and three starting at the poles. The smallest particles examined here, $\sigma = 2$, roam throughout the droplet and do not exhibit a preferred location. Increasing the particle size brings segregation toward the poles of the droplet.

To study the segregation dynamics, we follow the alignment of each particle's normalized position vector $\hat{\mathbf{r}}$ relative to the nematic ordering vector $\hat{\mathbf{n}}$ for the two largest particles considered here. The results are plotted in Figs. 2(b) and 2(c). Each particle exhibits a pronounced preference for the interfacial boojum defect. In the case of particles having $\sigma = 10$, particles placed at a polar region have a strong tendency to remain there, while particles placed at the equator segregate to the defect. This can be clearly seen in Fig. 2(c), where the green equatorial trajectories segregate toward the poles over the duration of a simulation despite slow diffusive motion of the particle in dense nematic LC. The polar trajectories retain configurations where the nematic axis is aligned with the particle position vector (though occasional fluctuations away from this alignment are observed). This behavior is suggestive of the presence of deep attractive wells for particles to the boojums.

In Fig. 2(d), we plot the free energy of interaction [or potential of mean force (PMF)], normalized by ε, between single particles and boojum defects for larger adsorbed colloids [17]. These simulations are performed at temperature $kT/\varepsilon = 1.44$, so the PMF may be converted to thermal units dividing by this factor. Here, the nematic director has been constrained to lie along the z axis, and bias is applied to sample particle positions along this axis. In agreement with the results in Fig. 2(a), we observe a monotonic deepening of the free-energy well with increasing particle size. Though small particles are ambivalent to their surroundings, significant free energetic gains of order several tens of $k_B T$ occur as particles are grown to the largest size considered here. As the origin of this free energetic, gain resides in the alleviation of elastic stress. Scaling our results to larger systems such as those amenable to experiment, we expect that only the elastic stress should play a role, as in the segregation of colloidal particles to nematic-isotropic phase boundaries [33]. Importantly, the minima observed for large particles are deep, and may be exploited for robust particle assembly.

Though in Fig. 1 we show the results of ideal two-particle placement, such robust assembly is not always the case. Indeed, as shown in Figs. 3(a)–3(d), particles often located near the same defect. As particles are themselves larger than a boojum, this is a suboptimal condition. To quantify this effect, in Fig. 3(e) we plot results of simulations for the free energy of two nanoparticles as a function of separation. These simulations proceed similarly to the one-particle calculations, except that here one particle is fixed in space at $z = 25$, and the nematic axis is free to reorient. This has the effect of fixing one particle at a boojum defect while the other particle is driven around the surface. In this case, the free energy exhibits two minima. Focusing on the free energy curve for $\sigma = 10$, the first minimum occurs when two particles share the same boojum defect, and has a depth of $\approx -25 k_B T$ relative to the maximum free energy for $\sigma = 10$ particles where we have utilized $k_B T/\varepsilon = 1.44$. This minimum develops as the nanoparticles are pushed close together, until it is mitigated by the repulsive interactions between

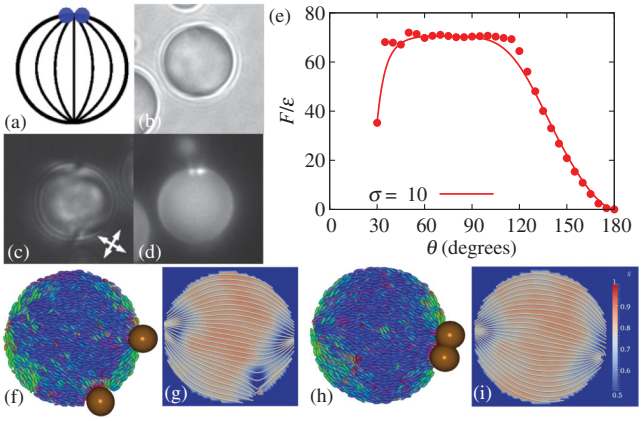

FIG. 3 (color). (a) Cartoon of two particles located at the same boojum defect, complemented by experimental images from bright-field (b), polarized-light (c), and fluorescence (d) microscopy. (e) Potential of mean force for two particles of size $\sigma = 10\sigma_0$ one of which is restricted to lie at the position of a boojum defect. The coordinate θ defines the angle between the particle's position vector (relative to the droplet center) and the nematic axis $\hat{\mathbf{n}}$. Two minima are observed, with particles either located near the same pole or segregating to opposing poles. The latter case is thermodynamically favorable for the large particle, as particle anchorings and steric effects prevent elastic relaxation within the droplet. Dots represent the computed potential, while the solid line is a Bezier curve approximation to the data. (f)–(i) Instantaneous morphology, order parameter maps, and field lines for two representative configurations of $\sigma = 10\sigma_0$ spheres. (f),(g) Particles separated by a 70° angle in the plane coincident with the droplet's center. The field lines in (g) show three defect regions, corresponding to the positions of the two particles and the free boojum. The region between the two particles is disordered relative to the bulk; this can be alleviated by the particle proceeding to the occupied boojum as in (h), or by migrating to the free boojum. (g),(h) Two particles sharing the same boojum defect. Interestingly, the field lines depicted in (i) appear to show an additional defect occupying the region between the two interacting particles.

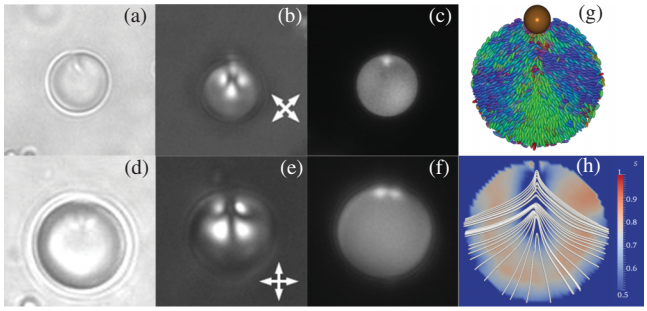

FIG. 4 (color). (a)–(c) Addition of 8 mM SDS to a droplet with one adsorbed particle results in a pinned preradial defect. Formation of this morphology is robust against the order of surfactant and particle adsorption. (d)–(f) The same method can be used to robustly select morphologies with two particles sharing the preradial defect. (g),(h) Simulations with an adsorbed nanoparticle ($\sigma = 10\sigma_0$) quenched from a radial morphology predict such a structure to occur at the transition from a bipolar to a radial droplet.

overlapping nanoparticles. In the cross-sectional view depicted in Fig. 3(h), one can see that the defect has been annihilated by the presence of the two particles. The second minimum occurs for particles at opposing boojums, and has depth $\approx 50k_BT$, comparable with the energy found in the one-particle case. The interior structure of the defect is modified when two particles are present at one pole, as evidenced by Fig. 3(i). The central repulsive region ($\theta \approx 90°$ in Fig. 3) contains contributions from strong elastic deformations of the nematic order, bringing the two boojum defects closer together, and from conformations where the driven nanoparticle has escaped the primary boojum, alleviating the elastic cost, but creating further stress associated with its surface anchoring. In metadynamics trajectories [17,34,35], we find that the boojum defect will detach when the particle is driven just past the equator of the droplet (taking the fixed particle and droplet center to define the polar axis). This observation correlates extremely well with the quantitative free energy results of Fig. 3(e), which show a plateau in the free energy when the droplet is near the equator, before presenting a strong second minimum for adjacent particles. This is further elucidated by Figs. 3(f) and 3(g), which show the two particles to interact through a region with nematic orientation which differs from the overall director, and which exhibits substantially more orientational disorder.

Finally, in Fig. 4, we consider the effects of droplet morphology on particle positioning. Here, surfactant [8 mM Sodium Dodecyl Sulfate (SDS)] is added to the aqueous dispersion to induce homeotropic anchoring on the droplet. Normally, this results in a radial droplet morphology. However, the presence of one [Figs. 4(a)–4(c)] or two [Figs. 4(d)–4(f)] particles pins the radial defect. This has the further effect of selecting a single two-particle arrangement from the two competing bipolar arrangements. A similar effect is predicted in simulations by preparing a radial state, and then adjusting the surface anchoring toward the bipolar–radial transition to mimic the addition of surfactant. Here, the radial defect moves from the center of the droplet to the surface and attaches preferentially to the nanoparticle. The presence of these stable states implies that a few adsorbed nanoparticles are sufficient to create morphological changes in LC droplets, which could be utilized in a reversible sequestration process.

The results reported in this Letter demonstrate the size-dependent segregation of nanoparticles to defect regions in LC droplets. While the droplet sizes examined here are small, past work has shown that they can be safely extrapolated to longer length scales, more amenable to experimental characterization [4,6]. The results reported here indicate that nematic droplets can indeed be used to create dipolar functional particles, where the particle on each pole could have different chemical characteristics, and thereby, offer unique possibilities for hierarchical assembly of ordered

structures. They also demonstrate that single particles can be used for active displacement of defects and release of a radial defect to an interface. Droplet formation is simple and robust, facilitating the creation of such particles in the laboratory. Extensions of these results to larger surface coverages by nanoparticles are underway.

The authors acknowledge support from the Department of Energy, Basic Energy Sciences, Biomaterials Program under Grant No. DE-SC0004025. J. K. W. was partially supported by a NHGRI training grant to the Genomic Sciences Training Program, No. T32HG002760. We gratefully acknowledge the computing resources provided on "Fusion," a 320-node computing cluster operated by the Laboratory computing Resource Center at Argonne National Laboratory. We acknowledge the University of Chicago Research Computing Center for use of the Midway cluster and support of this work. A portion of this research was performed using resources and the computing assistance of the UW-Madison Center For High Throughput Computing (CHTC), an active member of the Open Science Grid, which is supported by the National Science Foundation and the U.S. Department of Energy's Office of Science. J. K. W. acknowledges support from UChicago Argonne, LLC, Operator of Argonne National Laboratory ("Argonne"). Argonne, a U.S. Department of Energy Office of Science laboratory, is operated under Contract No. DE-AC02-06CH11357.

[1] R. Kamien, Rev. Mod. Phys. **74**, 953 (2002).
[2] J. K. Gupta, S. Sivakumar, F. Caruso, and N. L. Abbott, Angew. Chem., Int. Ed. Engl. **48**, 1652 (2009).
[3] S. I. Hernández, J. A. Moreno-Razo, A. Ramírez-Hernández, E. Díaz-Herrera, J. P. Hernández-Ortiz, and J. J. de Pablo, Soft Matter **8**, 1443 (2012).
[4] J. A. Moreno-Razo, E. J. Sambriski, N. L. Abbott, J. P. Hernández-Ortiz, and J. J. de Pablo, Nature (London) **485**, 86 (2012).
[5] M. J. Solomon, Curr. Opin. Colloid Interface Sci. **16**, 158 (2011).
[6] I.-H. Lin, D. S. Miller, P. J. Bertics, C. J. Murphy, J. J. de Pablo, and N. L. Abbott, Science **332**, 1297 (2011).
[7] D. Voloschenko, O. P. Pishnyak, S. V. Shiyanovskii, and O. D. Lavrentovich, Phys. Rev. E **65**, 060701 (2002).
[8] I. Muševič, M. Škarabot, D. Babič, N. Osterman, I. Poberaj, V. Nazarenko, and A. Nych, Phys. Rev. Lett. **93**, 187801 (2004).
[9] M. Škarabot, M. Ravnik, D. Babič, N. Osterman, I. Poberaj, S. Žumer, I. Muševič, A. Nych, U. Ognysta, and V. Nazarenko, Phys. Rev. E **73**, 021705 (2006).
[10] D. Pires, J.-B. Fleury, and Y. Galerne, Phys. Rev. Lett. **98**, 247801 (2007).
[11] J.-B. Fleury, D. Pires, and Y. Galerne, Phys. Rev. Lett. **103**, 267801 (2009).
[12] D. Coursault, J. Grand, B. Zappone, H. Ayeb, G. Lévi, N. Félidj, and E. Lacaze, Adv. Mater. **24**, 1461 (2012).
[13] M. Ravnik, G. P. Alexander, J. M. Yeomans, and S. Zumer, Faraday Discuss. **144**, 159 (2010).
[14] M. Ravnik, G. P. Alexander, J. M. Yeomans, and S. Žumer, Proc. Natl. Acad. Sci. U.S.A. **108**, 5188 (2011).
[15] D. S. Miller and N. L. Abbott, Soft Matter **9**, 374 (2013).
[16] A. Fernández-Nieves, V. Vitelli, A. S. Utada, D. R. Link, M. Márquez, D. R. Nelson, and D. A. Weitz, Phys. Rev. Lett. **99**, 157801 (2007).
[17] See Supplemental Material at http://link.aps.org/supplemental/10.1103/PhysRevLett.111.227801 for further information on experimental and simulation methodologies.
[18] J. G. Gay and B. J. Berne, J. Chem. Phys. **74**, 3316 (1981).
[19] E. de Miguel, L. F. Rull, M. K. Chalam, K. E. Gubbins, and F. Van Swol, Mol. Phys. **72**, 593 (1991).
[20] M. A. Bates and G. R. Luckhurst, J. Chem. Phys. **110**, 7087 (1999).
[21] D. J. Cleaver, C. M. Care, M. P. Allen, and M. P. Neal, Phys. Rev. E **54**, 559 (1996).
[22] M. P. Allen and D. J. Tildesley, *Computer Simulation of Liquids* (Oxford University Press, Oxford, 1987).
[23] F. F. Abraham and Y. Singh, J. Chem. Phys. **67**, 2384 (1977).
[24] D. Vanzo, M. Ricci, R. Berardi, and C. Zannoni, Soft Matter **8**, 11790 (2012).
[25] L. F. Rull, J. M. Romero-Enrique, and A. Fernández-Nieves, J. Chem. Phys. **137**, 034505 (2012).
[26] F. Mondiot, X. Wang, J. J. de Pablo, and N. L. Abbott, J. Am. Chem. Soc. **135**, 9972 (2013).
[27] E. B. Kim, O. Guzman, S. Grollau, N. L. Abbott, and J. J. de Pablo, J. Chem. Phys. **121**, 1949 (2004).
[28] The order parameter and field line maps in this Letter were created using PARAVIEW V. 3.98.1, published by Kitware, Inc. http://www.paraview.org.
[29] W. M. Brown, M. K. Petersen, S. J. Plimpton, and G. S. Grest, J. Chem. Phys. **130**, 044901 (2009).
[30] S. Plimpton, J. Comput. Phys. **117**, 1 (1995).
[31] J. N. Israelachvili, *Intermolecular and Surface Forces* (Academic Press, Waltham, MA, 2011), 3rd ed.
[32] R. Berardi, A. Costantini, L. Muccioli, S. Orlandi, and C. Zannoni, J. Chem. Phys. **126**, 044905 (2007).
[33] S. P. Meeker, W. C. K. Poon, J. Crain, and E. M. Terentjev, Phys. Rev. E **61**, R6083 (2000).
[34] A. Laio and F. L. Gervasio, Rep. Prog. Phys. **71**, 126601 (2008).
[35] S. Singh, M. Chopra, and J. J. de Pablo, Annu. Rev. Chem. Biomol. Eng. **3**, 369 (2012).